12th International Symposium on Turbulence and Shear Flow Phenomena (TSFP12)
Osaka, Japan (Online), July 19-22, 2022

WALL-ATTACHED STRUCTURES IN A TURBULENT CHANNEL FLOW WITH NAVIER SLIP

Min Yoon
Division of Mechanical Engineering
Korea Maritime and Ocean University
Busan 49112, Republic of Korea
minyoon@kmou.ac.kr

Hyung Jin Sung
Department of Mechanical Engineering
KAIST
Daejeon 34141, Republic of Korea
hjsung@kaist.ac.kr

ABSTRACT
We explore wall-attached structures in a drag-reduced turbulent channel flow with the Navier slip boundary condition. The three-dimensional coherent structures of the streamwise velocity fluctuations (u) are examined in an effort to assess the effects of wall-attached u structures on drag reduction. We extract the u clusters from the direct numerical simulation (DNS) data; for comparison, the DNS data for the no-slip condition are included. The wall-attached structures, which are physically adhere to the wall, in the logarithmic region are self-similar with their height and contribute to the presence of logarithmic behavior. The formation and hierarchy of wall-attached self-similar structures (WASS) are not affected by a streamwise slip, of which influences on them are limited up to the lower bound of logarithmic region, supporting Townsend's outer-layer similarity hypothesis. Weakened mean shear by the streamwise slip results in the decrease in the population density of wall-attached structures within the buffer layer. This leads to lower population of WASS, whereas the space occupied by them in the fluid domain increases. The conditional statistics are obtained to analyze the WASS in the vicinity of the wall. The streamwise slip induces long tails in the near-wall part of WASS, reminiscent of the footprints of large-scale motions. The present results reveal that the characteristics of WASS is irrespective of the streamwise slip and their near-wall part is main energy-containing motions.

INTRODUCTION
Townsend (1976) posited that the main energy-containing motions in the logarithmic region are self-similar with respect to their height (l_y) and attached to the wall. The attached-eddy hypothesis can be used to predict turbulence statistics through the construction of randomly superimposed attached eddies, and can be rigorously applied to an inviscid fluid near the wall for high-Reynolds-number turbulent flows. Perry and Chong (1982) extended Townsend's attached-eddy hypothesis to establish the attached eddy model by using a hierarchy of self-similar vortex eddies with population densities that are inversely proportional to their height. Recently, Hwang and Sung (2018) extracted wall-attached structures from the direct numerical simulation (DNS) data for a turbulent boundary layer; they reported that wall-attached structures of the streamwise velocity fluctuations (u) with an inverse power-law distribution contribute to the presence of the logarithmic region and are physically anchored to the wall. The near-wall turbulence is dominantly influenced by the viscosity and is closely related to the skin-friction reduction in drag-reduced flows (Min and Kim, 2004).

A strong shear layer is formed near the wall, which results in high skin friction in wall-bounded turbulence. Frictional drag adversely influences the efficiency and performance of engineering applications. Drag-reduced turbulent flows can be modeled by using the Navier slip boundary condition (Navier, 1823) in the streamwise direction (Min and Kim, 2004). Although many studies of turbulence statistics and structures in drag-reduced flows have been performed, not much attention has been paid to wall-attached structures, especially in the vicinity of the wall. Given that wall-attached structures are the main energy-containing motions in the logarithmic region and physically anchored to the wall, it is essential to establish the role of the roots of wall-attached structures in the frictional drag to understand the drag reduction mechanism.

NUMERICAL DETAILS
In the present study, the DNS data for turbulent channel flows with the Navier slip and no-slip boundary conditions of Yoon et al. (2016) were used. The Navier−Stokes equations and continuity equation for an incompressible flow were discretized by using the fractional step method (Kim et al. 2002). The bulk Reynolds number (Re_b) is equivalent to 10,333. The Navier slip boundary condition was applied in the streamwise direction, i.e. $\tilde{u}_S = L_S(\mathrm{d}\tilde{u}/\mathrm{d}y)|_{\mathrm{wall}}$, where $\tilde{u}_S$ is the slip velocity, L_S is the slip length, $\tilde{u}$ is the streamwise velocity, and y is the wall-normal location. The slip length is fixed at 0.01δ to give a drag reduction rate of 35% for the channel flow with the no-slip condition. Here, δ is the channel half-height. The friction Reynolds numbers (Re_τ) for the slip and no-slip cases are 469 and 577, respectively. The characteristics of the computational domain are summarized in Table 1, where x and z are the streamwise and spanwise directions, respectively. The superscript "+" denotes quantities normalized by the wall units of each case.

Table 1. Parameters of the computational domain and friction Reynolds number. L_i and N_i are domain sizes and the number of grids in each direction, respectively. $\Delta y_{\min}^+$ and $\Delta y_{\max}^+$ denote resolutions of the first grid from the wall and the grid at the channel half-height, respectively.

	Slip	No-slip
L_x/δ	10π	10π
L_z/δ	3π	3π
N_x	2,497	2,497
N_y	401	401
N_z	1,249	1,249
Δx^+	5.92	7.27
Δz^+	3.55	4.36
$\Delta y_{\min}^+$	0.08	0.10
$\Delta y_{\max}^+$	5.96	7.32
Re_τ	469	577

RESULTS

Figure 1 represents the turbulence statistics for the slip and no-slip cases. The magnitude of streamwise mean velocity (U^+) is larger than that of no-slip case due to the streamwise slip. The dashed line in figure 1(a) exhibits the mean velocity relative to the wall ($U^+ - U_S^+$) for the slip case, which coincides with the profile of U^+ for the no-slip case. The mean shear (dU^+/dy^+) is insensitive to the streamwise slip. The streamwise slip induces a virtual origin in U^+ at $y^+ = -Ls^+$, leading to the upward shift of U^+ as $\Delta U^+ = U_S^+ = L_S^+$ in the entire region (García–Mayoral et al., 2019).

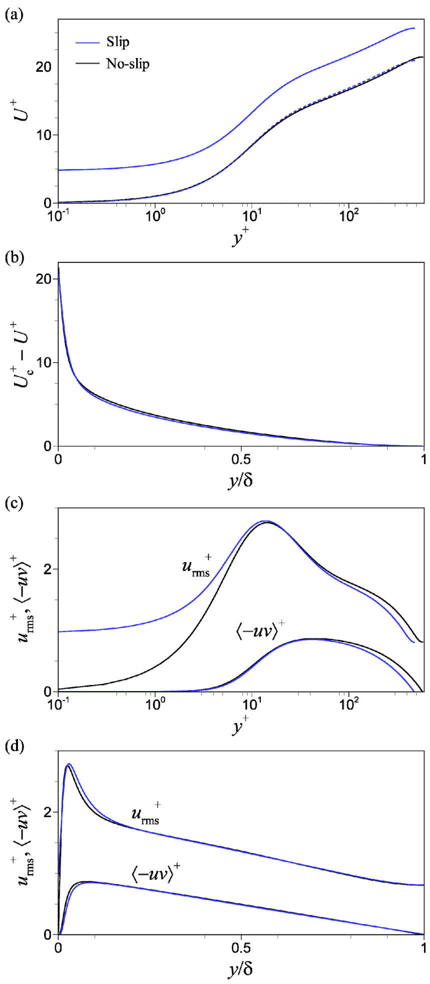

Figure 1. Profiles of (a) mean velocity and (b) defect form of mean velocity. A dashed line in (a) represents mean velocity relative to wall for slip case. Profiles of streamwise turbulence intensity (u_{rms}^+) and Reynolds shear stress ($\langle -uv\rangle^+$) for (c) inner scaling and (d) outer scaling.

The magnitude of streamwise turbulence intensity (u_{rms}^+) is amplified in $y^+ < 10$, especially very close to the wall (figure 1c), due to the streamwise slip. On the contrary, the profile of Reynolds shear stress ($\langle -uv\rangle^+$) is well matched with that for the no-slip case in the inner region as a result of an impermeable condition at the wall. For outer scaling, the profiles of $U_c^+ - U^+$, u_{rms}^+ and $\langle -uv\rangle^+$ for both cases collapse well in the outer region, supporting Townsend's outer-layer similarity hypothesis. This observation is a good agreement with results of Flores and Jiménez (2006) and Chung et al. (2014). Here, U_c is the mean velocity at the channel center.

The 3-D u clusters in instantaneous flow fields can be defined as the groups of connected points satisfying $u \geq \alpha u_{rms}$ and $u \leq -\alpha u_{rms}$, where α is the threshold. The threshold can be chosen from the percolation diagram in figure 2. The total number (N) and total volume (V) of clusters at a given α are normalized by the maximum N (N_{max}) and maximum V (V_{max}), respectively. As α decreases, new clusters arise, or some adjacent clusters merge. The peak in N/N_{max} at $\alpha = 1.6$ results from the tradeoff between these two influences. In addition, V/V_{max} increases as the decrease in α with strong variation in $1.4 < \alpha < 1.8$, where the percolation transition occurs. Hence, we adopted $\alpha = 1.6$ in the present study.

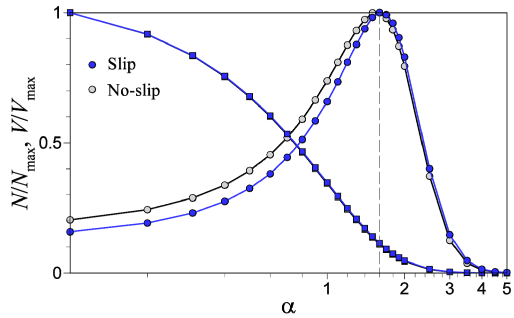

Figure 2. Variations with α in the total volume (V) (square) and total number (N) (circle) of clusters.

Each cluster can be identified based on above condition by using the connectivity of six-orthogonal grids at a given node in Cartesian coordinates (Moisy and Jiménez, 2004). As a result, the spatial information about each cluster can be obtained. The clusters with volumes less than 30^3 wall units are deleted to avoid grid resolution (del Álamo et al., 2006). Figure 3 shows the population density (n^*) of all the identified clusters with respect to y_{max} and y_{min}, which are the maximum and minimum distances from the wall, respectively. Here, n^* is defined as the number of u clusters (n) per unit wall-parallel area ($A_{xz} = L_xL_z$), i.e. $n^* = n(y_{max}, y_{min})/(mA_{xz})$, where m is the number of snapshots. Two distinct groups are evident at $y_{min}^+ \approx 0$ and $y_{min}^+ > 0$. The former are wall-attached structures, and the latter are wall-detached structures (Hwang and Sung, 2018).

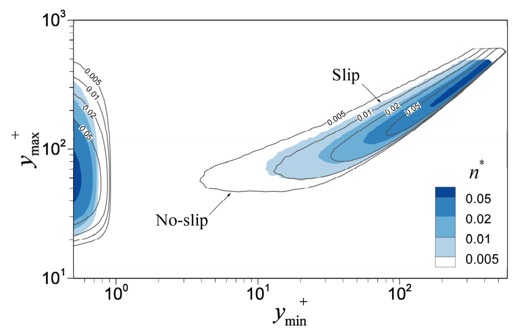

Figure 3. The number of u clusters per unit wall-parallel area (n^*) with respect to y_{min}^+ and y_{max}^+.

Figure 4 illustrates the 3-D iso-surfaces of u of wall-attached structures for the slip case. Green and gold represent negative u and positive u, respectively. The characteristic lengths of each cluster are defined in terms of the dimensions of the box circumscribing the object. The inset in figure 4 shows a sample and its length scales, i.e. l_x, l_z and l_y, which are the streamwise and spanwise sizes and the height, respectively. The wall-attached structures are coherent in the streamwise direction, and they are aligned side by side in the spanwise direction.

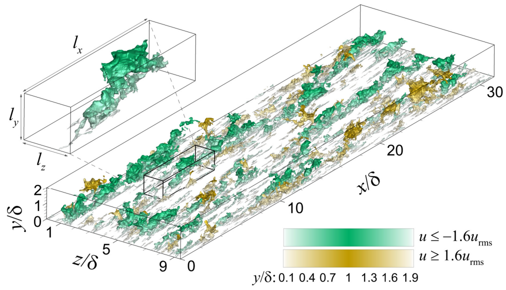

Figure 4. 3-D iso-surfaces of the wall-attached u structures in an instantaneous flow field for the slip case.

Figure 5 shows the mean l_x^+ ($\langle l_x^+\rangle$) and mean l_z^+ ($\langle l_z^+\rangle$) with respect to l_y^+, which is the height of wall-attached structures, for the slip (blue) and no-slip (grey) cases. The mean l_x^+ is proportional to l_y^+ with the power of 0.74 (Hwang and Sung, 2018) in $l_y^+ \geq 70 \approx 3Re_\tau^{0.5}$, whereas not proportional to l_y^+ in $l_y^+ < 70$. Here, $3Re_\tau^{0.5}$ is the lower limit of logarithmic region (Marusic et al., 2013; Hwang and Sung, 2019), which accords with approximately $70\nu/u_\tau$ at the present Reynolds number, $Re_\tau \approx 500$. In addition, there is a linear relationship between the mean l_z^+ and l_y^+ ($l_y^+ \geq 70$), showing that the spanwise size of wall-attached u structures is proportional to the distance from the wall (Tomkins and Adrian, 2003; Hwang, 2015). In particular, the profiles of $\langle l_x^+\rangle$ and $\langle l_z^+\rangle$ for both cases coincide in the entire l_y^+, especially $l_y^+ \geq 70$, in agreement with the results of Lozano–Durán and Bae (2019). Accordingly, we divide wall-attached structures into non-self-similar ($l_y^+ < 70$) and self-similar ($l_y^+ \geq 70$) structures.

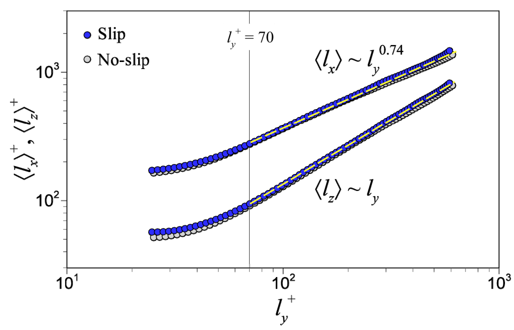

Figure 5. The mean l_x^+ and mean l_z^+ of wall-attached u structures. The yellow lines represent $\langle l_x\rangle \sim l_y^{0.74}$ and $\langle l_z\rangle \sim l_y$, respectively.

The population density (n_a^*) of wall-attached structures as a function of l_y^+ is shown in figure 6. Here, n_a is the number of wall-attached structures at a given l_y, and n_a^* is defined as n_a per unit wall-parallel area, i.e. $n_a^* = n_a/(mA_{xz})$. The magnitude of n_a^* is smaller than that for the no-slip case in the entire region. The wall-attached structures with $l_y^+ = O$ (10) are related to near-wall streaks. As shown in figure 1, the mean shear is preserved near the wall for the slip case, sustaining turbulence via the formation process of streaky structures (Hamilton et al., 1995). The streamwise slip attenuates streamwise vortices near the wall, creating streaks sparsely (Min and Kim, 2004). The lack of streamwise vortices leads to reduced populations of wall-attached structures near the wall.

The magnitude of n_a^* is inversely proportional to l_y^+ in $250 < l_y^+ < 400$ for both cases, reminiscent of the distribution of hierarchy length scales of attached eddies (Perry and Chong, 1982). The inverse power-law dependence arises within the region of $l_y^+ = 0.3\delta^+$–$0.6\delta^+$ (Hwang and Sung, 2018; Hwang and Sung, 2019). The streamwise slip induces a decrease in the population density of wall-attached structures, but the inverse power law is still valid. The no-slip boundary condition is not indispensable to form hierarchical distributions of wall-attached structures. In addition, a peak in n_a^* arises at $l_y^+ = 1.06\delta^+$ for both cases, which attributes the large population of wall-attached δ-height structures (Perry et al., 1986).

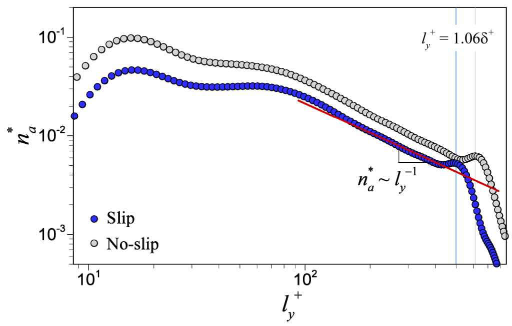

Figure 6. Population density (n_a^*) of wall-attached structures as a function of l_y^+. Red line denotes an inverse power-law distribution of n_a^*.

Figure 7 shows wall-normal profiles of streamwise Reynolds stresses ($\langle uu\rangle_a^{*+}$) carried by the wall-attached structures with $l_y^+ = 300$,

$$\langle uu\rangle_a^* = \left\langle S_a(y, l_y)^{-1}\int_{S_a} u(\mathbf{x})u(\mathbf{x})\mathrm{d}x\mathrm{d}z\right\rangle, \qquad (1)$$

where S_a is the wall-parallel area of wall-attached structures. The magnitude of $\langle uu\rangle_a^{*+}$ for $l_y^+ = 300$ is logarithmically proportional to y^+ ($\langle uu\rangle_a^{*+} \sim \ln y^+$) in $100 < y^+ < 220$ (Perry and Chong, 1982). Although the present Reynolds number is relatively low ($Re_\tau \approx 500$), the logarithmic variation is evident in $\langle uu\rangle_a^{*+}$ (Hwang and Sung, 2018; Hwang and Sung, 2020; Yoon et al., 2020). The logarithmic behavior of wall-attached structures is sustained regardless of the streamwise slip at the wall.

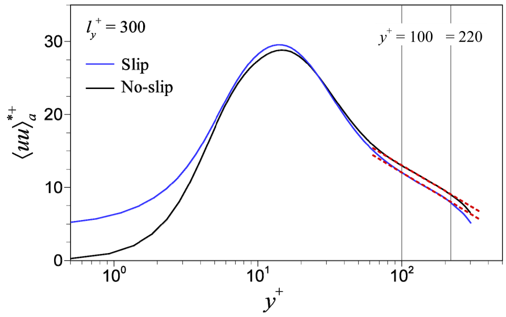

Figure 7. Streamwise Reynolds stresses ($\langle uu \rangle_a^+$) reconstructed by wall-attached structures with the height of $l_y^+ = 300$. Red dashed lines indicate the best fits in $100 < y^+ < 220$.

The characteristics of wall-attached structures can be decomposed into buffer-layer ($l_y^+ < 70 \approx 3Re_\tau^{0.5}$) and self-similar ($l_y^+ \geq 70$) structures. The upper part ($y^+ \geq 70$) of wall-attached self-similar structures (WASS) ($l_y^+ \geq 70$) is responsible for the logarithmic behavior (figure 7). The near-wall part ($y^+ < 70$) of WASS ($l_y^+ \geq 70$) contributes to geometrical self-similarity. The wall-attached structures can be divided into $u_{\rm nws}$, $u_{\rm uws}$ and $u_{\rm wb}$, which are defined as

$$u_{\rm nws} = \begin{cases} u & \text{if } |u| \geq 1.6u_{\rm rms},\ y^+_{\min} \approx 0,\ y^+_{\max} \geq 70,\ y^+ < 70, \\ 0 & \text{otherwise,} \end{cases} \tag{2}$$

$$u_{\rm uws} = \begin{cases} u & \text{if } |u| \geq 1.6u_{\rm rms},\ y^+_{\min} \approx 0,\ y^+_{\max} \geq 70,\ y^+ \geq 70, \\ 0 & \text{otherwise,} \end{cases} \tag{3}$$

$$u_{\rm wb} = \begin{cases} u & \text{if } |u| \geq 1.6u_{\rm rms},\ y^+_{\min} \approx 0,\ y^+_{\max} < 70, \\ 0 & \text{otherwise.} \end{cases} \tag{4}$$

Here, the subscripts 'nws', 'uws' and 'wb' represent the near-wall part of WASS, upper part of WASS and wall-attached buffer-layer structures (WABS), respectively. We focus on the near-wall part of WASS, in which the viscosity effect is dominant.

To investigate characteristic lengths of the near-wall part of WASS statistically, conditional two-point correlations of $u_{\rm nws}$ are examined at the reference wall-normal location $y_{\rm ref}^+ = 14.5$, where the inner peak appears in $u^+_{\rm rms}$ (figure 1c). The two-point correlation of $u_{\rm nws}$ is defined as,

$$R[u_{\rm nws}, u_{\rm nws}] = \frac{\langle u_{\rm nws}(x, y_{\rm ref}, z) u_{\rm nws}(x + r_x, y, z + r_z) \rangle}{u_{\rm nws,rms}(y_{\rm ref}) u_{\rm nws,rms}(y)}, \tag{5}$$

where $u_{\rm nws,rms}$ is the root-mean-square quantity of $u_{\rm nws}$.

Wall-parallel views of $R[u_{\rm nws}, u_{\rm nws}]$ are displayed in figure 8. Solid and dashed lines correspond to 5% of the maximum of positive $R[u_{\rm nws}, u_{\rm nws}]$ and 50% of the minimum of negative $R[u_{\rm nws}, u_{\rm nws}]$, respectively. The positive $R[u_{\rm nws}, u_{\rm nws}]$ are extended over 4δ in the streamwise direction, which is similar to streamwise lengths of the footprints of large-scale motions at $y^+ \approx 14.5$ (Hwang et al., 2016). In addition, the negative $R[u_{\rm nws}, u_{\rm nws}]$ indicates that the near-wall part of WASS is aligned side by side along the spanwise direction. The distance to the center (cross symbol) of negative $R[u_{\rm nws}, u_{\rm nws}]$ at $r_x/\delta = 0$ is 0.6δ, which is 20% larger than that for the no-slip case. It represents that the near-wall part of WASS is more sparsely distributed than those for the no-slip case.

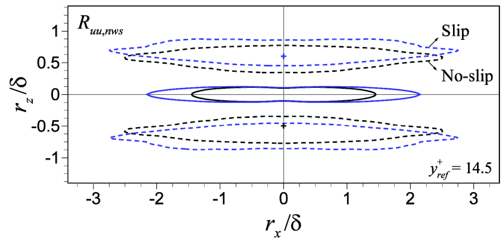

Figure 8. Two-point correlations of u_{nws}. Solid lines represent 5% of the maximum of positive correlations, and dashed lines denote 50% of the minimum of negative correlations. Cross symbols indicate spanwise centers of negative correlations.

We scrutinize the turbulence statistics of the near-wall part of WASS with respect to y. The turbulence statistics carried by the near-wall part of WASS are conditionally averaged based on conditional fields, where velocity fluctuations are obtained using equations similar to (2). Conditionally averaged quantities are used to assess contributions of the near-wall part of WASS to the turbulence statistics in $y^+ < 70$.

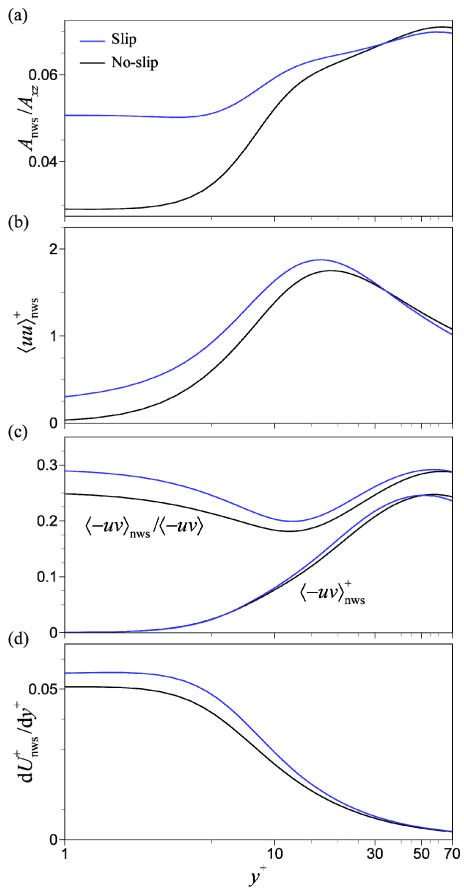

Figure 9. Conditionally averaged turbulence statistics of the near-wall part of WASS: wall-normal profiles of (*a*) $A_{\rm nws}/A_{xz}$, (*b*) $\langle uu \rangle^+_{\rm nws}$, (*c*) $\langle -uv \rangle^+_{\rm nws}$, and (*d*) $dU^+_{\rm nws}/dy^+$.

Figure 9 shows wall-normal profiles of conditional averages for the near-wall part of WASS. Profiles of A_{nws}/A_{xz} represent wall-parallel areas occupied by the near-wall part of WASS, which account for 5 ~ 7% of the area of the x–z plane. Below $y^+ = 30$, the magnitude of A_{nws}/A_{xz} is larger than that for the no-slip case, in particular, approximately 75% larger near the wall. As shown in figure 9(b), the magnitude of $\langle uu\rangle^+_{\mathrm{nws}}$ is larger than that for the no-slip case below $y^+ = 30$. The near-wall part of WASS is strengthened by the streamwise slip.

The profiles of $\langle -uv\rangle^+_{\mathrm{nws}}$ for both cases collapse (figure 9c), similar to $\langle -uv\rangle^+$. The near-wall part of WASS carries approximately 30% of total $\langle -uv\rangle$ in spite of small A_{nws}/A_{xz} as the main energy-containing motions near the wall. Figure 9(d) represents the mean shear ($\mathrm{d}U^+_{\mathrm{nws}}/\mathrm{d}y^+$) carried by the near-wall part of WASS. Below $y^+ = 20$, the magnitude of $\mathrm{d}U^+_{\mathrm{nws}}/\mathrm{d}y^+$ is larger than that for the no-slip case, especially by 9% close to the wall. The magnitude of $\mathrm{d}U_{\mathrm{nws}}{}^+/\mathrm{d}y^+$ at the wall can be arranged to the ratio $\tau_{w,\mathrm{nws}}/\tau_w$. Here, $\tau_{w,\mathrm{nws}}$ is the wall shear stress carried by the near-wall part of WASS. Given that the wall shear stress is related to the skin friction coefficient (Fukagata et al., 2002), the high $\mathrm{d}U_{\mathrm{nws}}{}^+/\mathrm{d}y^+$ at the wall is responsible for the frictional drag. The mean shear of the near-wall part of WASS for the slip case is restored over $y^+ = 30$. The near-wall part of WASS is varied by the viscosity and wall conditions, but their contributions to the streamwise Reynolds stress and Reynolds shear stress are more significant.

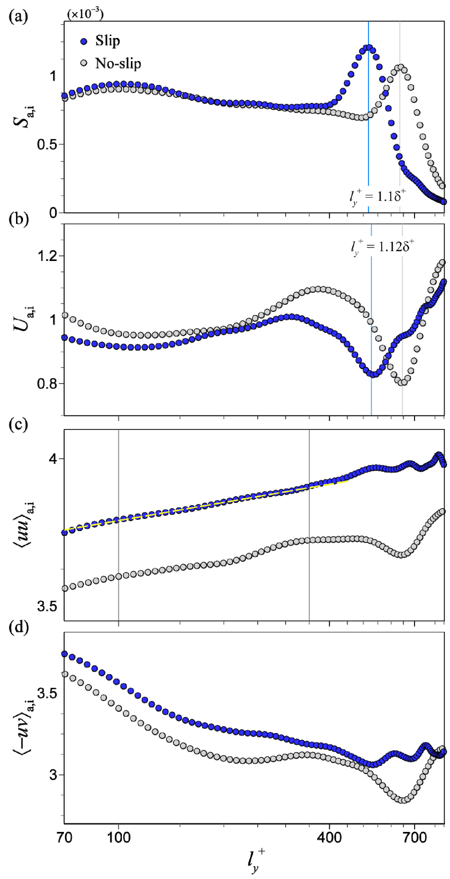

Figure 10. Conditional averages of the near-wall part of WASS at $y^+ = 14.5$: (*a*) $S_{\mathrm{a,i}}$ (*b*) $U_{\mathrm{a,i}}$, (*c*) $\langle uu\rangle_{\mathrm{a,i}}$, and (*d*) $\langle -uv\rangle_{\mathrm{a,i}}$. A green line in (*c*) denotes the logarithmic variation.

To explore the characteristics of the near-wall part of WASS with respect to l_y at the near-wall region, conditional averages of wall-parallel area, streamwise velocity, streamwise Reynolds stress and Reynolds shear stress are examined at $y^+ = 14.5$. They are defined as,

$$S_{\mathrm{a,i}} = S_{\mathrm{a}}(y,l_y)|_{y^+=14.5}/(mA_{xz}), \tag{6}$$

$$U_{\mathrm{a,i}} = U^*_{\mathrm{a}}(y,l_y)|_{y^+=14.5}/U(y)|_{y^+=14.5}, \tag{7}$$

$$\langle uu\rangle_{\mathrm{a,i}} = \langle uu\rangle^*_{\mathrm{a}}(y,l_y)|_{y^+=14.5}/\langle uu\rangle(y)|_{y^+=14.5}, \tag{8}$$

$$\langle -uv\rangle_{\mathrm{a,i}} = \langle -uv\rangle^*_{\mathrm{a}}(y,l_y)|_{y^+=14.5}/\langle -uv\rangle(y)|_{y^+=14.5}. \tag{9}$$

Figure 10(a) shows profiles of the areas in the x–z plane ($S_{\mathrm{a,i}}$) occupied by the near-wall part of WASS at $y^+ = 14.5$. The magnitude of $S_{\mathrm{a,i}}$ gradually decreases as the increase in l_y^+ with a peak at $l_y^+ = 1.1\delta^+$. The quantities of $U_{\mathrm{a,i}}$, $\langle uu\rangle_{\mathrm{a,i}}$ and $\langle -uv\rangle_{\mathrm{a,i}}$ describe the dependence on l_y in their contributions to the turbulence statistics (i.e. U, $\langle uu\rangle$ and $\langle -uv\rangle$) at $y^+ = 14.5$. Figure 10(b) represents profiles of $U_{\mathrm{a,i}}$ with respect to l_y^+. The region of l_y^+, where the magnitude of $U_{\mathrm{a,i}}$ is larger than 1, indicates that positive u of the near-wall part of WASS at given l_y^+ is dominant near $y^+ = 14.5$, and *vice versa*. A concave peak of $U_{\mathrm{a,i}}$ is evident at $l_y^+ = 1.12\delta^+$. In particular, the profile of $U_{\mathrm{a,i}}$ is shifted downward from that for the no-slip case, especially in $l_y^+ = 300$–δ^+. It shows that the population of wall-attached negative-u structures with $l_y^+ \approx \delta^+$ are more dominant than that for the no-slip case (Yoon et al., 2016).

The streamwise Reynolds stress ($\langle uu\rangle_{\mathrm{a,i}}$) at $y^+ = 14.5$ is shown at figure 10(c). The magnitude of $\langle uu\rangle_{\mathrm{a,i}}$ gradually increases as l_y^+ increases. The contributions of the near-wall part of WASS to the streamwise Reynolds stress are enhanced as increasing l_y^+. In particular, the magnitude of $\langle uu\rangle_{\mathrm{a,i}}$ is logarithmically proportional to l_y^+ in $100 < l_y^+ < 350$ ($\langle uu\rangle_{\mathrm{a,i}} \sim \ln l_y^+$) (a yellow line). The inner-peak magnitude of streamwise Reynolds stress logarithmically increases with increasing Re_τ (Jiménez and Hoyas, 2008; Marusic et al., 2017). Since l_y is related to hierarchical scales (figure 7), the logarithmic variation in $\langle uu\rangle_{\mathrm{a}}$ with respect to l_y reflects hierarchical features of wall-attached structures (Hwang and Sung, 2018). The logarithmic variation in $\langle uu\rangle_{\mathrm{a}}$ is evident in $200 < l_y^+ < 300$. A hierarchy of wall-attached structures is well established over the broader range of l_y. Figure 10(d) shows profiles of $\langle -uv\rangle_{\mathrm{a,i}}$, of which the value is larger than 3 in $l_y^+ < \delta^+$. It means that the near-wall part of WASS carry three times more Reynolds shear stresses than $\langle -uv\rangle$ in the near-wall region ($y^+ = 14.5$). The magnitude of $\langle -uv\rangle_{\mathrm{a,i}}$ is larger than that for the no-slip case below $l_y^+ = \delta^+$. These observations imply that the contributions of the near-wall part of WASS to the near-wall turbulence are dominant, since the Reynolds shear stress is directly related to turbulent contributions to the skin friction coefficient (Fukagata et al., 2002).

CONCLUSIONS

We have explored wall-attached u structures in a drag-reduced turbulent channel flow and demonstrated their contributions to near-wall turbulence. We extracted 3-D u clusters by using the connectivity of six-orthogonal neighbors in Cartesian coordinates from the DNS dataset for turbulent channel flows with a Navier slip wall ($Re_\tau = 470$) and no-slip wall ($Re_\tau = 577$). We showed that wall-attached structures are formed in their entirety in instantaneous flow fields on the wall with the streamwise slip. The wall-attached structures with $l_y^+ \geq 70 \approx 3Re_\tau^{0.5}$ were self-similar with l_y, and their geometrical features remained unchanged regardless of the streamwise slip. The hierarchical distribution with an inverse power law and the logarithmic behavior of WASS ($l_y^+ \geq 70$) were not influenced by the streamwise slip. Influences of the streamwise slip on the wall-attached structures were limited up to the lower bound ($y^+ = 3Re_\tau^{0.5}$) of logarithmic region. The streamwise slip induced the decrease in the population density of WABS ($l_y^+ < 70$) with weakened mean shear. The decrease in the population density of WASS is attributed to that of WABS, whereas the space occupied by WASS in the fluid domain is enlarged. In addition, we have focused on the near-wall part ($y^+ < 70$) of WASS. The conditional average and conditional fields were employed. The near-wall part of WASS was extended in the streamwise direction over 4δ, reminiscent of the footprints of large-scale motions. The near-wall part of WASS contributed to approximately 30% of the Reynolds shear stress. The Reynolds shear stress carried by the near-wall part of WASS is enhanced by the streamwise slip. The streamwise slip curtails the population density of WASS. The present study enhances our understanding of the behavior of wall-attached structures and furthers the development of attached-eddy models of drag-reduced flows.

ACKNOWLEDGMENTS

This work was supported by the National Research Foundation of Korea (NRF) grant funded by the Korea government (MSIT) (No. 2020R1A2C2008106 and 2021R1F1A1053438).

REFERENCES

del Álamo, J. C., Jiménez, J., Zandonade, P., and Moser, R. D., 2006, "Self-similar vortex clusters in the turbulent logarithmic region", *Journal of Fluid Mechanics*, Vol. 561, pp. 329–358.

Chung, D., Monty, J. P., and Ooi, A., 2014, "An idealised assessment of Townsend's outer-layer similarity hypothesis for wall turbulence", *Journal of Fluid Mechanics*, Vol. 742, R3.

Flores, O., and Jiménez, J., 2006, "Effect of wall-boundary disturbances on turbulent channel flows", *Journal of Fluid Mechanics*, Vol. 566, pp. 357–376.

Fukagata, K., Iwamoto, K., and Kasagi, N., 2002, "Contribution of Reynolds stress distribution to the skin friction in wall-bounded flows", *Physics of Fluids*, Vol. 14(11), L73–L76.

García–Mayoral, R., Gómez–de–Segura, G., and Fairhall, C. T., 2019, "The control of near-wall turbulence through surface texturing", *Fluid Dynamics Research*, Vol. 51(1), 011410.

Hamilton, J. M., Kim, J., and Waleffe, F., 1995, "Regeneration mechanisms of near-wall turbulence structures", *Journal of Fluid Mechanics*, Vol. 287, pp. 317–348.

Hwang, J., Lee, J., Sung, H. J., and Zaki, T. A., 2016, "Inner-outer interactions of large-scale structures in turbulent channel flow", *Journal of Fluid Mechanics*, Vol. 790, pp. 128–157.

Hwang, J., and Sung, H. J., 2018, "Wall-attached structures of velocity fluctuations in a turbulent boundary layer", *Journal of Fluid Mechanics*, Vol. 856, pp. 958–983.

Hwang, J., and Sung, H. J., 2019, "Wall-attached clusters for the logarithmic velocity law in turbulent pipe flow", *Physics of Fluids*, Vol. 31(5), 055109.

Hwang, J., Lee, J. H., and Sung, H. J., 2020, "Statistical behavior of self-similar structures in canonical wall turbulence", *Journal of Fluid Mechanics*, Vol. 905, A6.

Hwang, Y., 2015, "Statistical structure of self-sustaining attached eddies in turbulent channel flow", *Journal of Fluid Mechanics*, Vol. 767, pp. 254–289.

Jiménez, J., and Hoyas, S., 2008, "Turbulent fluctuations above the buffer layer of wall-bounded flows", *Journal of Fluid Mechanics*, Vol. 611, pp. 215–236.

Kim, K., Baek, S. J., and Sung, H. J., 2002, "An implicit velocity decoupling procedure for the incompressible Navier–Stokes equations", *International journal for numerical methods in fluids*, Vol. 38(2), pp. 125-138.

Lozano–Durán, A., and Bae, H. J., 2019, "Characteristic scales of Townsend's wall-attached eddies", *Journal of Fluid Mechanics*, Vol. 868, pp. 698–725.

Marusic, I., Baars, W. J., and Hutchins, N., 2017, "Scaling of the streamwise turbulence intensity in the context of inner-outer interactions in wall turbulence", *Physical Review Fluids*, Vol. 2(10), 100502.

Marusic, I., Monty, J. P., Hultmark, M., and Smits, A. J., 2013, "On the logarithmic region in wall turbulence", *Journal of Fluid Mechanics*, Vol. 716, R3.

Min, T., and Kim, J., 2004, "Effects of hydrophobic surface on skin-friction drag", *Physics of Fluids*, Vol. 16(7), L55–L58.

Moisy, F., and Jiménez, J., 2004, "Geometry and clustering of intense structures in isotropic turbulence", *Journal of fluid mechanics*, Vol. 513, pp. 111–133.

Navier, C. L. M. H., 1823, "Mémoire sur les lois du mouvement des fluids", *Mémoires de l'Académie Royale des Sciences de l'Institut de France*, Vol. 6, pp. 389–440.

Perry, A. E., and Chong, M. S., 1982, "On the mechanism of wall turbulence", *Journal of Fluid Mechanics*, Vol. 119, pp. 173–217.

Perry, A. E., Henbest, S., and Chong, M. S., 1986, "A theoretical and experimental study of wall turbulence", *Journal of Fluid Mechanics*, Vol. 165, pp. 163–199.

Tomkins, C. D., and Adrian, R. J., 2003, "Spanwise structure and scale growth in turbulent boundary layers", *Journal of Fluid Mechanics*, Vol. 490, pp. 37–74.

Townsend, A. A., 1976, *The structure of turbulent shear flow*, Cambridge university press.

Yoon, M., Hwang, J., Lee, J., Sung, H. J., and Kim, J., 2016, "Large-scale motions in a turbulent channel flow with the slip boundary condition", *International Journal of Heat and Fluid Flow*, Vol. 61, pp. 96–107.

Yoon, M., Hwang, J., Yang, J., and Sung, H. J., 2020, "Wall-attached structures of streamwise velocity fluctuations in an adverse pressure gradient turbulent boundary layer", *Journal of Fluid Mechanics*, Vol. 885, A12.